

Article

Long-Range Influence of Cr on the Stacking Fault Energy of Cr-Containing Concentrated Solid-Solution Alloys

Hao Xiao ¹ , Qingyuan Liu ¹ , Shijun Zhao ² , Songqin Xia ¹, Yugang Wang ¹ and Chenxu Wang ^{1,*} 

¹ State Key Laboratory of Nuclear Physics and Technology, Peking University, Beijing 100871, China

² Department of Mechanical Engineering, City University of Hong Kong, Hong Kong, China

* Correspondence: cxwang@pku.edu.cn

Abstract: Single-phase concentrated solid-solution alloys (CSAs) have exhibited excellent mechanical and radiation tolerance properties, making them potential candidate materials for nuclear applications. These excellent properties are closely related to dislocation movements, which depend on the stacking fault energies (SFEs). In CSAs, SFEs show large fluctuations due to variations in the local atomic environments in the vicinity of the stacking faults. In this work, first-principle calculations were performed to investigate the origin of the fluctuations in the SFEs of the widely studied CSA, NiCoCr, which show a very wide distribution from about -200 mJ/m^2 to 60 mJ/m^2 . Compared to the common understanding that only atoms in close proximity to the stacking fault influence the SFEs in pure metals and dilute alloys, charge redistribution can be observed in several nearby planes of the stacking fault in NiCoCr, indicating that atoms several atomic layers away from stacking fault also contribute to the SFEs. Our analysis shows that Cr plays a major role in the large fluctuation in the SFEs of NiCoCr based on both electronic and magnetic responses. The flexible electronic structure of Cr facilitates easier charge transfer with Cr in several nearby atomic planes near the stacking fault, leading to significant changes in the *d*-electron number, orbital occupation number, and magnetic moments of Cr.

Keywords: concentrated solid-solution alloys; stacking fault energy; first-principle calculations; electronic structure



Citation: Xiao, H.; Liu, Q.; Zhao, S.; Xia, S.; Wang, Y.; Wang, C. Long-Range Influence of Cr on the Stacking Fault Energy of Cr-Containing Concentrated Solid-Solution Alloys. *Metals* **2024**, *14*, 560. <https://doi.org/10.3390/met14050560>

Academic Editor: Cristian Ciobanu

Received: 10 March 2024

Revised: 26 April 2024

Accepted: 5 May 2024

Published: 10 May 2024



Copyright: © 2024 by the authors. Licensee MDPI, Basel, Switzerland. This article is an open access article distributed under the terms and conditions of the Creative Commons Attribution (CC BY) license (<https://creativecommons.org/licenses/by/4.0/>).

1. Introduction

Single-phase concentrated solid-solution alloys (CSAs) with two or more multiple principal elements have attracted widespread attention due to their excellent mechanical properties, corrosion resistance, and radiation tolerance [1–6]. In particular, NiCoFeCrMn, a Ni-based CSA, exhibits outstanding fracture toughness and exceptional damage tolerance under tensile stress, especially at cryogenic temperatures [3], which inspires researchers' investigation on Ni-based CSAs including two to five principal elements [7–9]. As a typical example of a Cantor alloy derivative, NiCoCr shows even better strength–toughness properties, with a tensile strength of 1.4 GPa, a ductility of 90%, and a fracture strength of $275 \text{ MPa/m}^{1/2}$ at 77 K [10]. It has been proved experimentally that these excellent mechanical properties are closely related to the change of the deformation mechanism from conventional dislocation gliding to more nano-twinning with decreasing temperature [3,11–14]. In addition, many studies have shown that NiCoCr exhibits excellent radiation resistance. Jin et al. [15] irradiated NiCoCr up to 53 displacements per atom (dpa) at 500 °C using 3.0 MeV Ni ions and found that the irradiation swelling rate of NiCoCr (0.2%) was significantly slower than that of pure Ni (6.7%). Granberg et al. [6] irradiated NiCoCr with Ni and Au ions with the energies of 1.5 and 3 MeV and found a substantial reduction in damage accumulation under prolonged irradiation in single-phase NiCoCr alloys compared to elemental Ni. It is commonly believed that one of the reasons accounting for the good radiation resistance of CSAs is their atomic-level heterogeneity, which causes point-to-point local lattice distortion

and suppresses the dislocation slipping and defect cluster growth [16]. These results indicate that the dislocation motion plays an important role in the properties of CSAs. It is known that the deformation mechanism and dislocation motion in fcc alloys greatly depend on the stacking fault energy (SFE) [17–19]. In general, deformation twinning is energetically favorable when the SFE is low, while dislocation gliding is favored with a high SFE. The low SFE can also lead to deformation-induced phase transformation from fcc to hcp phase due to the low value of $\Delta E_{\text{fcc}-\text{hcp}}$ [20]. This demonstrates that the SFE is an important indicator of the material properties of CSAs.

The SFE in NiCoCr has been investigated in many studies through both experiments and first-principle calculations [12,13,19,21–23], which show a very wide distribution from about -200 mJ/m^2 to 60 mJ/m^2 . This large fluctuation in the SFEs results from the variations in the local atomic configurations in the CSAs [21,22]. It has been proved that the fluctuation in the SFEs of CSAs is closely related to their mechanical properties. Prior experimental studies have demonstrated that the observed fluctuation of the dislocation line [24], which is due to the fluctuation in the SFEs, impedes dislocation motion and thus enhances the mechanical strength of the CSAs [25]. Atomistic simulations show that the critical stress to activate dislocation motion is much higher in CSAs compared to that in pure Ni, due to this significant fluctuation in the SFEs [26]. Zhao showed that the large fluctuation can effectively suppress defect numbers and defect cluster growth under accumulated cascade conditions, thus enhancing the radiation resistance [27]. Therefore, the large fluctuation in the SFEs of CSAs has a profound impact on their properties.

In CSAs, the atomic structure is characterized by different elements occupying the sites of the lattice in a nonperiodic manner. In the simplest description, multiple elements are randomly distributed in a single lattice. However, local chemical order, i.e., ordering in the first few neighboring atomic shells to enhance the number of energetically preferred bond types has been observed in experiments. Zhang et al. [28] found that the Cr atoms are favorably bonded with Ni and Co in NiCoCr using neutron total scattering and extended X-ray absorption fine structure techniques. Similarly, Zhang et al. [29] found that Cr-Cr pairs are strongly disfavored at nearest-neighbor distances in NiCoCr using energy-filtered transmission electron microscopy. The SFE of NiCoCr increases with increasing amounts of such order and can be tuned by tailoring the local chemical order through thermomechanical processing [19,29]. In addition, radiation-induced segregation has been observed in several Ni-based CSAs including NiCoCr, in which Ni tends to enrich near defect clusters (loops and voids) due to chemically preferential diffusion [30–33]. The short-range order and radiation-induced segregation will change the local atomic environments and the fluctuation in the SFEs. Therefore, understanding the origin of the SFEs' fluctuation can help to predict the evolution of materials' properties during either the thermomechanical process or the irradiation process.

For CSAs comprising 3d transition metals, such as NiCoCr, 3d electrons play a key role in determining the peculiar performance of the CSAs. For example, it was found that defect migration can be understood by considering the inhomogeneous electronic charge distribution through charge transfer between e_g and t_{2g} states [34], which are two energy levels split from d orbitals according to energy and symmetry. The semi-filled 3d electrons of Cr are used to illustrate the magnetic frustration in NiCoCr, which leads to easier fcc-hcp phase transformation and contributes to enhanced strength [23]. The electronic effect of the SFEs of CSAs has also been reported. Atomistic simulations found that local variations in the SFEs of CSAs correlate with the charge density redistribution in the stacking fault region, which can be described quantitatively by a bond breaking and forming model [22]. However, this model, which considers the bonds in the first nearest neighboring plane of the stacking fault, fits well for NiCo but not as well for NiFe and NiCoCr, especially for NiCoCr. Therefore, further electronic analysis is needed to explore the factors that affect the SFE variations of NiCoCr.

In this work, first-principle calculations based on density functional theory (DFT) were employed to investigate the origin of the large fluctuation in the SFEs of NiCoCr. The SFEs

of Ni, NiFe, and NiCoCr were calculated and compared, showing that the stacking fault in NiCoCr had a longer influence distance. By constructing two specific situations, Cr was verified to dominate the significant fluctuation in the SFEs of NiCoCr. Furthermore, *d*-electron numbers, orbital occupation numbers in t_{2g} and e_g orbitals, and magnetic moments were used to capture the characteristics of Cr. Our results help to understand the electronic effects in stacking fault structures and the important role of the specific atoms on the significant fluctuations in the SFEs of CSAs.

2. Methods

DFT calculations were implemented using the Vienna ab initio simulation package (VASP) code [35]. A gradient-corrected functional in the Perdew–Burke–Ernzerhof (PBE) form was used to describe the exchange and correlation interactions [36]. Electron–ion interactions were treated within the projector-augmented-wave (PAW) method [37], and the standard PAW pseudopotentials provided by VASP were used. First-order Methfessel and Paxton smearing of the Fermi surface was used [38], with a smearing width of 0.1 eV. The *I*-quantum number was set to 4 to account for *d*-element behavior precisely. The energy cutoff for the plane-wave basis set was 400 eV. The energy convergence was set to be 10^{-4} eV. Spin-polarized calculations were carried out in all calculations.

To construct the chemical disorder structures of the CSAs, the special quasi-random structure (SQS) method [39,40] was used in the Alloy Theoretic Automated Toolkit code (ATAT) [41]. The lattice parameters were obtained by fitting the calculated energy–volume relation to the B-M equations in 108-atom bulk samples. The SQSs were cleaved to slab structures oriented in the [112], [110], and [110] directions with 12 atoms on each [111] plane. The number of layers ranged from 7 to 17. A vacuum layer with a thickness of greater than 20 Å was added. The thickness of the vacuum layer was tested to avoid its impact on the SFE for the surface atoms on either side of the vacuum layer will interact with each other and cause changes in electronic and magnetic properties if the vacuum layer is thin. It was found that even 20 Å was not enough for NiCoCr with 15 and 17 layers, in which case 30 Å was used. An intrinsic stacking fault was introduced by rigidly shifting the upper half [111] layers in the [112] directions, as shown in Figure 1a. The Brillouin zone was sampled with a $4 \times 4 \times 1$ K-mesh using a gamma-centered scheme. The energy cutoff and K-mesh were sufficiently tested to ensure an error of less than 1 meV/atom. The atomic positions were relaxed only along [111] by minimizing the Hellmann–Feynman forces on each atom to less than 10^{-2} eV/Å. When calculating the DOS, the energy convergence was increased to 10^{-7} eV with a $6 \times 6 \times 2$ K-mesh, and the tetrahedron method with Blöchl corrections was used. Finally, the SFE was calculated by the formula [42]:

$$\gamma_{SF} = \frac{1}{A}(E_{SF} - E_0) \quad (1)$$

where A is the area of stacking fault and E_{SF} and E_0 are the energy of the structures with and without stacking fault, respectively.

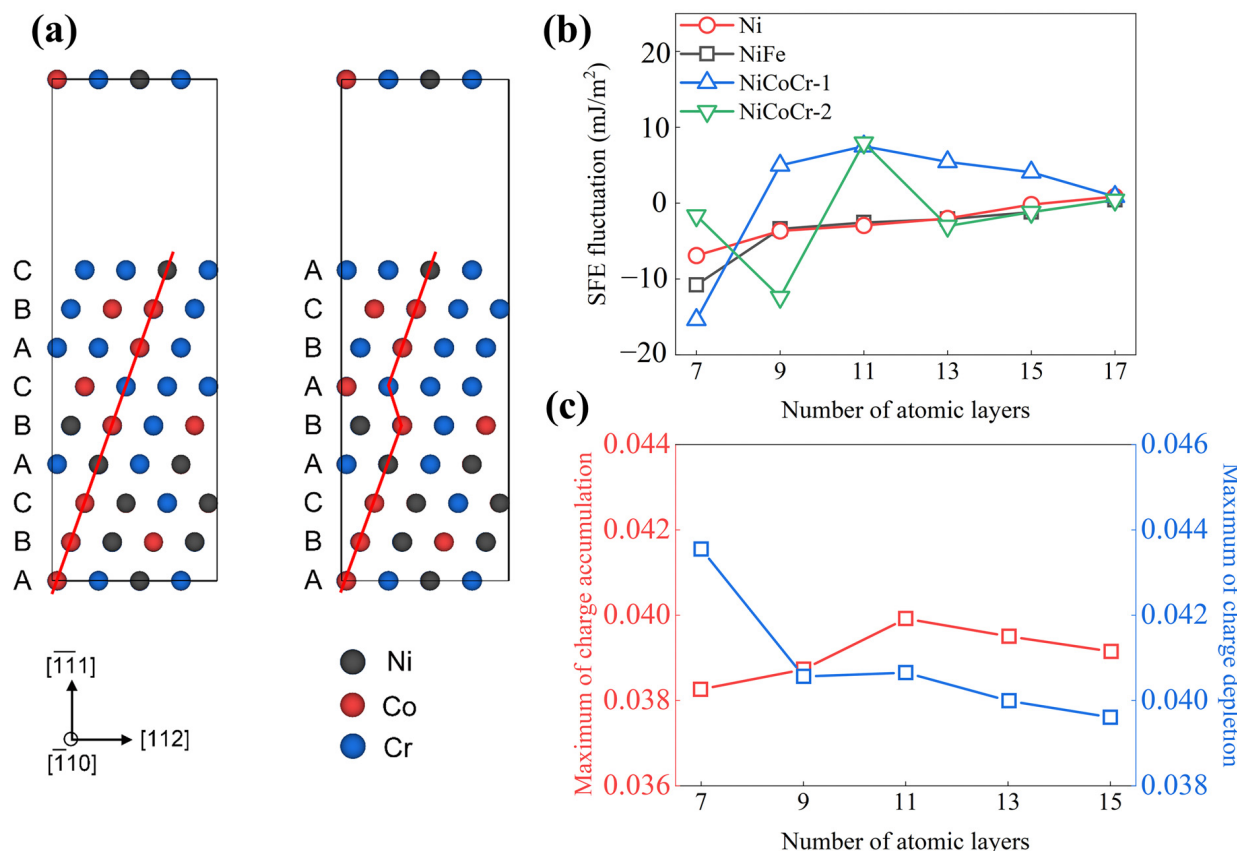


Figure 1. (a) The atomic configurations before and after introducing a stacking fault. (b) SFE fluctuation of Ni, NiFe, and NiCoCr with different layers. (c) The maximum accumulation and maximum depletion of charge on the stacking fault center surface of the NiCoCr with an increase in the number of atomic layers. Compared to Ni and NiFe, longer-range atomic layers in NiCoCr affect the SFE.

3. Results and Discussion

Firstly, pure Ni was investigated to verify the calculation methods. The lattice parameter of pure Ni, obtained from the fitting of the energy–volume relation using B-M equations, was 3.517 Å, which is similar to 3.522 Å in previous work [43]. The SFE of pure Ni calculated in this work was 130 mJ/m², which is within the range of 120–142 mJ/m² reported in the previous study [21]. This good agreement indicates that the calculation method is reliable. The calculated lattice parameters and SFEs of NiFe and NiCoCr are listed in Table 1. These lattice parameters are all comparable to those in the references. It is worth mentioning that the SFEs of NiFe and NiCoCr had very wide ranges, different from pure metals and dilute alloys. Especially in NiCoCr, the range was from −200 to 60 mJ/m². It has been proved that the fluctuation in the SFE is closely related to the stacking fault area used in calculations, and the standard deviation (σ) of the SFE distribution decreases as the area increases using empirical potential calculations [22]. In the limit of an infinite stacking fault area, σ will be zero and the SFE is a single value. However, the stacking fault area of alloys is finite in reality, so different SFEs, related to the local atomic configurations, are expected. The different SFEs mean that the mechanical properties of the material may vary at different locations.

Table 1. Calculated lattice parameters and SFEs of Ni, NiFe, and NiCoCr in this work. The lattice parameters from references are listed for comparison. CASs show large fluctuations in their SFEs.

	Lattice Parameter (Å)		SFE (mJ/m ²)
	This Work	Reference	This Work
Ni	3.517	3.522 [43]	130
NiFe	3.574	3.583 [44]	0–200
NiCoCr	3.527	3.529 [21]	−200–60

The SFE of alloys strongly depends on their local atomic environments. In general, for dilute alloys, only atoms on the nearest neighboring atomic layer of the stacking fault will contribute to the SFE [45]. However, large fluctuations in magnetic moments have been observed in the third nearest neighboring atomic layer and even in more distant atomic layers of NiFe and NiCoCr alloys [22], suggesting that more distant atoms in both alloy systems also contribute to the SFE. To investigate the range of atomic arrangement that plays a role in the SFE in concentrated solid-solution alloys, the central atomic arrangement of the stacking fault remained unchanged, and new atomic layers were added to the top and bottom of the stacking fault, respectively, to examine whether the external atoms still contributed to the SFE. Figure 1b shows the SFE fluctuations of Ni, NiFe, and NiCoCr with the atomic layers ranging from 7 to 17. The SFE for the 17-atomic-layer structure was stabilized, so the SFE fluctuations were defined as the SFE differences between the 17 atomic layer structure and other different atomic layer structures. It can be observed from Figure 1b that the SFEs of Ni and NiFe stayed stable as there were more than seven atomic layers. However, the SFEs of NiCoCr still underwent significant changes as the atomic layers increased up to 13 layers.

It has been proved that the stacking faults lead to charge redistribution in the stacking fault region [22,46–48]. Before and after the introduction of stacking faults, the charge density in the region near the stacking faults changes significantly, and the connection between charge density at bond critical points and SFE has been established [22]. The investigation of charge redistribution is an effective way to illustrate the fluctuation in the SFEs. Therefore, we calculated the maximum accumulation and depletion of charge on the stacking fault's center surface of NiCoCr with the increasing number of atomic layers, as shown in Figure 1c. The results show different degrees of charge transfer on the stacking fault center surface up to 13 atomic layers, which is consistent with the results of the change in the SFE. The atoms at the sixth nearest neighbor atomic layer (6 nnp) still affected the SFEs of NiCoCr alloys. The diversity of atomic configurations in the 6 nnp range led to large variations in the SFEs of NiCoCr alloys.

The average values of the absolute values of the changes in magnetic moments μ of the different atoms on each nearby plane before and after the introduction of the stacking faults were also calculated for the Ni, NiFe, and NiCoCr alloys, as shown in Figure 2. In pure Ni, the variation in magnetic moments was mainly concentrated within 1 nnp, and in NiFe, the variation in magnetic moments was mainly concentrated within 2 nnp. In contrast, in NiCoCr, there were significant variations in the magnetic moments of both Co and Cr up to 3 nnp, especially for Cr, which still had a variation in the magnetic moment at 6 nnp. This consistency between the results of the SFEs and the charge redistribution suggests that Cr atoms may play an important role in the variation of the SFEs.

To further analyze the role of Cr on SFE fluctuations, the electronic structures were analyzed in terms of electronic density of states (DOS) and charge density distribution. For alloys composed of transition metal elements, the DOS is dominated by d electrons [34,49,50]. Figure 3 shows the result for the projected DOS (PDOS) of Ni, Co, and Cr atoms in 1 nnp before and after introducing a stacking fault. The t_{2g} and e_g orbitals are two components of d electrons based on symmetries. It can be observed from Figure 3 that the PDOS changed for all three atoms after the introduction of a stacking fault. This is because the bonds between the upper and lower half parts are broken and rebuilt after the introduction of

the stacking fault. Compared to Ni and Co, the change was more significant in Cr, with a significant increase in the occupation of t_{2g} states and a decrease in e_g states near the Fermi level. Table 2 shows the d -electron occupation in t_{2g} and e_g orbitals for the three atoms in the perfect structures and the stacking fault structures. It should be noted that $\Delta(t_{2g})$ and $\Delta(e_g)$ are usually positive and negative, respectively, and their sum may not be zero, indicating that the charge transfer occurs not only between the t_{2g} and the e_g orbitals but also between different atoms. The differences in t_{2g} and e_g values for Ni and Co were relatively small, while the differences were larger for Cr, with 0.06 for t_{2g} and -0.03 for e_g . Another aspect of the investigation into the charge transfer at stacking fault is the calculation of the charge density difference before and after the introduction of the stacking fault. As shown in Figure 4, the charge density difference for Cr was more significant as well as more complex than that for Co and Ni. The charge density difference near Cr can be as high as 0.13 e/bohr 3 and has both positive and negative values along different directions asymmetrically. Combined with the DOS and charge density difference, the charge redistribution induced by the stacking fault in NiCoCr mainly occurred in Cr.

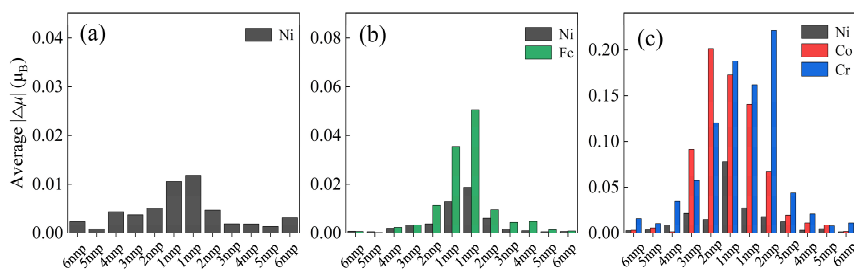


Figure 2. The average values of the absolute values of magnetic moment changes in each neighboring plane of the stacking fault in (a) Ni, (b) NiFe, and (c) NiCoCr.

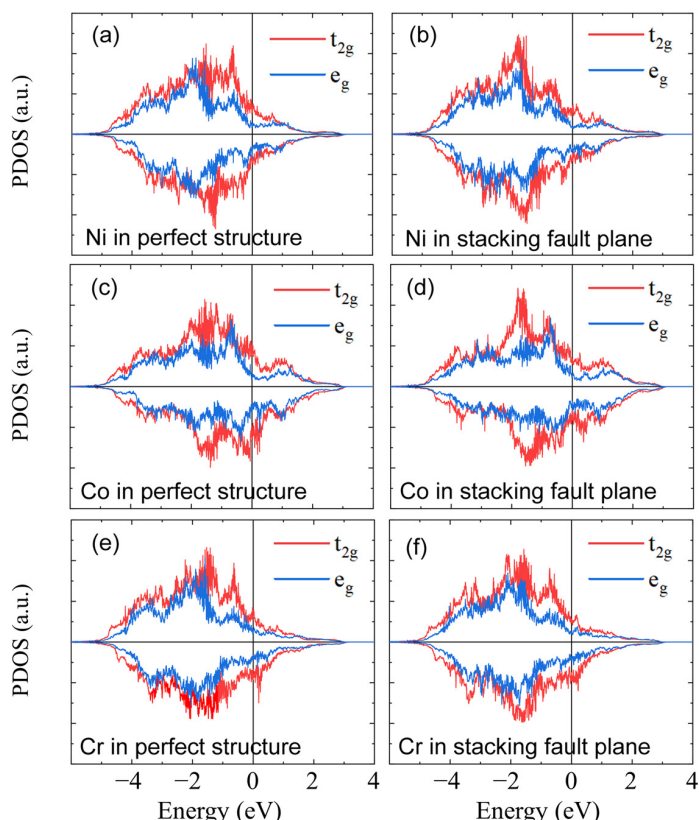


Figure 3. A typical example of PDOS of (a,b) Ni, (c,d) Co, and (e,f) Cr atom in 1 nnp before and after introducing a stacking fault. Compared to Ni and Co, the change in Cr is more significant.

Table 2. The d -electron occupation in t_{2g} and e_g orbitals for the three constituent elements in NiCoCr in the perfect structures and the stacking fault (SF) structures.

	Perfect Structure		SF Structure		Difference	
	t_{2g}	e_g	t_{2g}	e_g	$\Delta(t_{2g})$	$\Delta(e_g)$
Ni	5.03	3.28	5.02	3.29	−0.01	0.01
Co	4.41	2.92	4.38	2.93	−0.03	0.01
Cr	2.47	1.69	2.53	1.66	0.06	−0.03

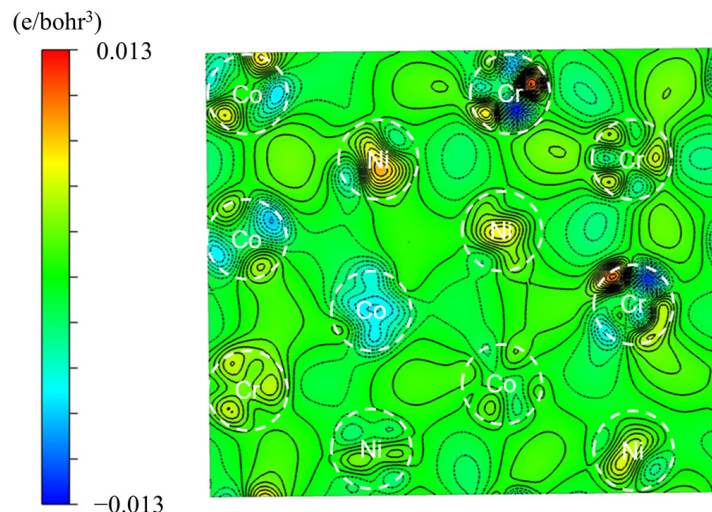


Figure 4. The charge density difference of 1 nnp of stacking fault on the $[1\bar{1}\bar{1}]$ plane before and after the introduction of stacking fault. The charge density difference for Cr is more significant as well as more complex than that for No and Ni.

To further demonstrate the influence of Cr on SFE fluctuations in NiCoCr, we constructed two scenarios for comparison. In scenario one, as shown in Figure 5a, NiCoCr was randomly distributed in the middle six layers and more NiCo layers were added to the outside, while in scenario two, as shown in Figure 5b, NiCo was in the middle and more NiCoCr layers were added to the outside. In this way, Cr was isolated either in the inner layers or in the outer layers. Three configurations were calculated for each scenario. The influence of the addition of different atomic layers on the SFE in these two scenarios is shown in Figure 5c and 5d, respectively. When the added atomic layer included Cr, there was a significant change in the SFE, whereas there was only a small change in the SFE when the added atomic layer contained only Ni and Co. This result clearly indicates that Cr atoms, even five atomic layers away from the stacking fault, still impacted the SFEs compared to Ni and Co.

Furthermore, we calculated the changes in the occupation number of the t_{2g} and e_g orbitals for each element near the stacking fault in each scenario before and after the introduction of a stacking fault. Figure 5e shows the average of $|\Delta(t_{2g})|$ and $|\Delta(e_g)|$ for each element in 1 nnp of stacking fault in Configuration 1, and Figure 5f shows the average of $|\Delta(t_{2g})|$ and $|\Delta(e_g)|$ for Ni and Co in 1 nnp of stacking fault and Cr in 4 nnp in Configuration 4. When adding Ni and Co in the outer layers, the SFE, as well as the t_{2g} and e_g values, did not change significantly. However, when adding Cr in the outer layers, the SFE changed significantly, accompanied by substantial changes in the electronic structures of Cr as shown in Figure 5f. This correspondence clearly indicates that the fluctuation in Figure 5d is attributed to the change in the electronic structures of Cr.

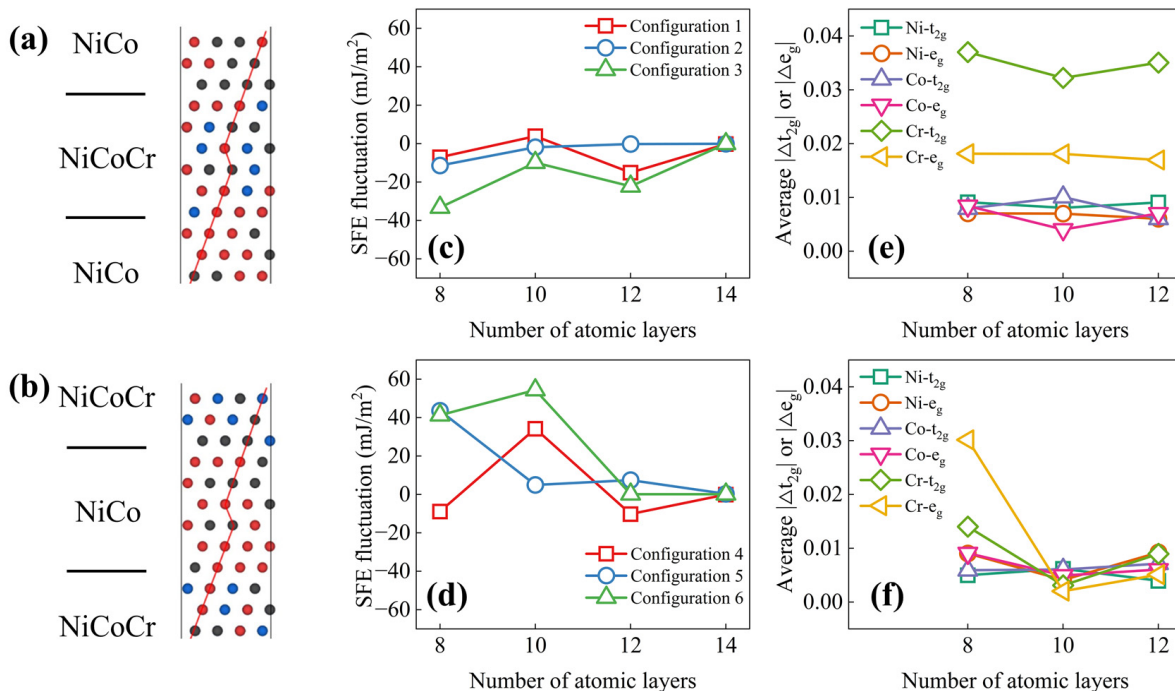


Figure 5. The schematic diagram of NiCoCr in the inner layer (**a**) and the outer layer (**b**). The influence of adding atomic layers on the SFE fluctuation with NiCoCr in the inner layer (**c**) and outer layer (**d**). The influence of adding atomic layers on electronic structures with NiCoCr in the inner layer (**e**) and the outer layer (**f**).

In addition, we considered the cases in which SFE is negative, close to 0, and positive, respectively. Three 12-layer configurations were calculated to investigate the different electronic and magnetic responses of the three constituent elements to the stacking fault. As shown in Figure 6, in all three cases, the t_{2g} and e_g orbital electrons of Cr exhibited significant changes after the introduction of the stacking fault compared to those of Ni and Co. Correspondingly, the number of d electrons and the magnetic moment of Cr likewise changed most significantly. The results further underscore the dominant role of Cr in the fluctuations in the SFEs.

Due to its semi-filled valence electrons, Cr possesses a more flexible electronic structure than Ni and Co. Consequently, more charge transfer occurs with Cr, resulting in changes in the d -electron number, orbital occupation number, and also magnetic moments. On the contrary, Ni and Co have almost full valence electrons, thus they only need to make small adjustments to accommodate changes in their immediate neighbor, i.e., Cr. When changes occur in the arrangement of Cr in the stacking fault structure of NiCoCr, the charge transfer and magnetic moment will change significantly, leading to a change in the SFE that ranges from -200 mJ/m^2 to 60 mJ/m^2 . Moreover, a long range of Cr atoms contribute to this process. As a result, the diverse charge redistribution due to the differences in the atomic arrangement of Cr over a wide range is the key factor that influences the variation in the SFE of NiCoCr.

Radiation-induced elemental segregation in Ni-based CSAs has been reported in many studies. Using Ni ions to irradiate Ni, NiCo, NiFe, NiCoCr, NiCoFe, and CoCrFeNi CSAs at room temperature, Tuomisto et al. [30] concluded that elemental segregation occurred at a very low irradiation damage level in the CSAs by positron annihilation spectroscopy analyses. Lu et al. [31] irradiated a group of single-phase CSAs, NiFe, NiCoFe, NiCoFeCr, and NiCoFeCrMn using 3 MeV Ni²⁺ ions at 773 K and found that Ni and Co tend to enrich, while Cr, Fe, and Mn prefer to deplete near the defect clusters. Considering the crucial role of Cr in the large fluctuations in the SFEs, the depletion of Cr in NiCoCr will likely lead to a smaller fluctuation in the SFEs under irradiation, and the average of the SFEs

may approach that of NiCo, potentially detrimentally affecting the mechanical properties of NiCoCr. Moreover, the degree of local ordering at the nanometer scale can be tailored through thermomechanical processing in CSAs. Given Cr's important role for SFEs, the focus of regulating local ordering may concentrate on the distribution of Cr. Our work enhances the understanding of the effects of specific elements on the SFEs of CSAs.

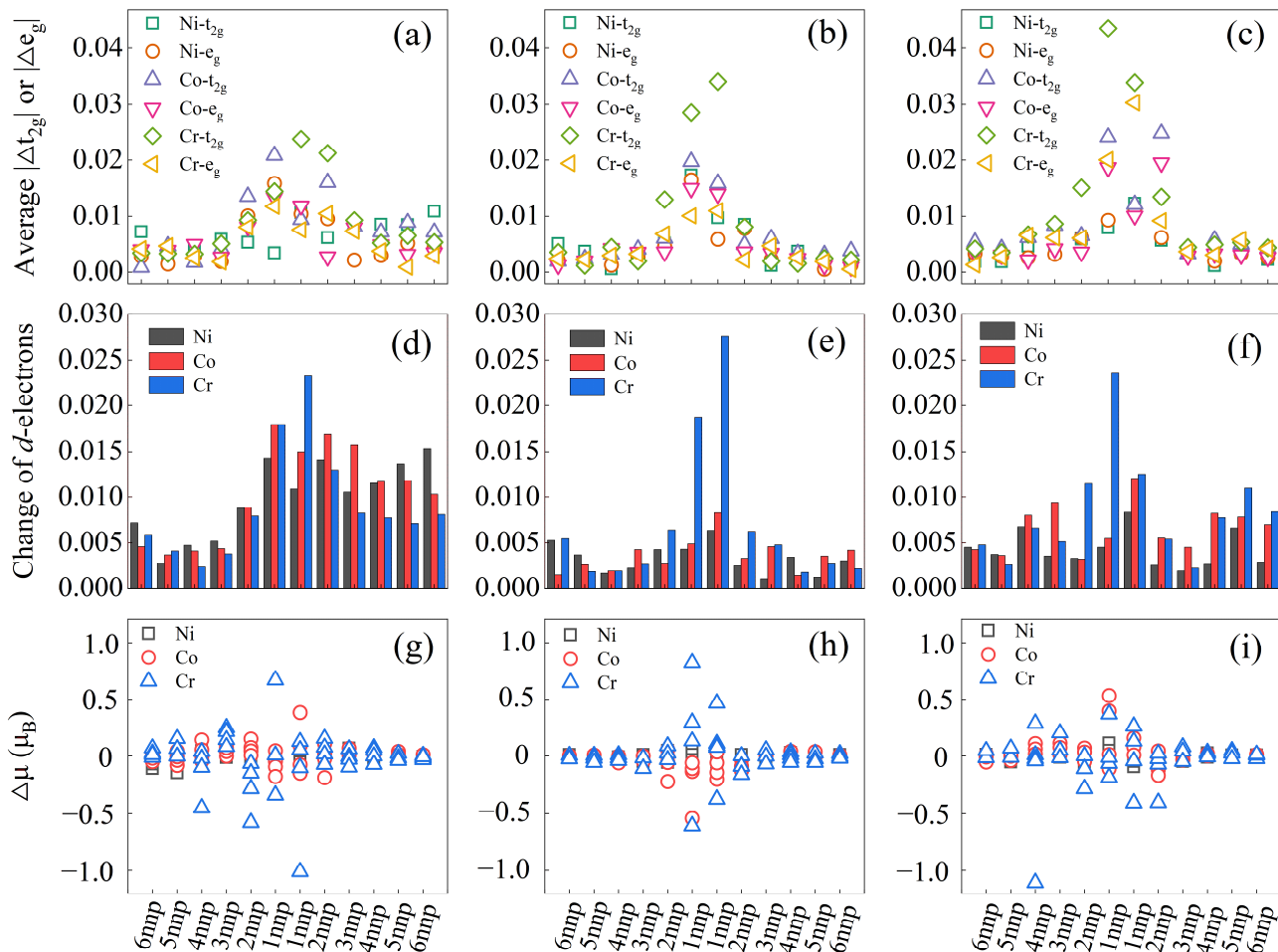


Figure 6. Changes in the electronic structures (a–c), number of *d*-electrons (d–f), and magnetic moments (g–i) in each neighboring plane for negative, close to zero, and positive SFE values. In all three cases, Cr shows the largest change in the three quantities.

4. Conclusions

In this work, we investigated the large fluctuations in the stacking fault energy of NiCoCr concentrated solid-solution alloys with a range from -200 mJ/m^2 to 60 mJ/m^2 by first-principle calculation. By constructing two special situations, it was found that the Cr element plays an important role in the fluctuation of the SFEs. Due to the complex electronic structure of Cr, when the arrangement of Cr atoms near the stacking fault is varied, it will lead to significant changes in the charge distribution, such as the t_{2g} and e_g orbital electrons, thus changing the SFE. In particular, a long range of Cr arrangements can affect the SFE. Our results help to understand the role of element-specific electronic structures, particularly those elements with half-filled electron shells, on the stacking fault structure in CSAs.

Author Contributions: Conceptualization, Q.L., S.Z., Y.W. and C.W.; Methodology, H.X., Q.L. and S.Z.; Software, H.X. and Q.L.; Validation, Y.W., C.W. and S.X.; Formal analysis, H.X. and Q.L.; Investigation, Q.L., S.X. and C.W.; Resources, Y.W. and C.W.; Data curation, H.X. and Q.L.; Writing—original draft preparation, H.X. and Q.L.; Writing—review and editing, C.W., S.Z. and H.X.; Visualization, H.X. and

Q.L.; Supervision, Y.W.; Project administration, Y.W. and C.W.; Funding acquisition, Y.W. and C.W. All authors have read and agreed to the published version of the manuscript.

Funding: This research was funded by the National Natural Science Foundation of China (Grant Nos. 12275009, 11935004, and 12192280) and the National Magnetic Confinement Fusion Energy Research Project 2021YFE031100.

Data Availability Statement: The original contributions presented in the study are included in the article/supplementary material, further inquiries can be directed to the corresponding author/s.

Acknowledgments: The authors are grateful for the computing resources provided by the High-Performance Computing Platform of the Center for Life Science (Peking University).

Conflicts of Interest: The authors declare no conflict of interest.

References

- Yeh, J.W.; Chen, S.K.; Lin, S.J.; Gan, J.Y.; Chin, T.S.; Shun, T.T.; Tsau, C.H.; Chang, S.Y. Nanostructured High-Entropy Alloys with Multiple Principal Elements: Novel Alloy Design Concepts and Outcomes. *Adv. Eng. Mater.* **2004**, *6*, 299–303. [[CrossRef](#)]
- Chen, Y.Y.; Duval, T.; Hung, U.D.; Yeh, J.W.; Shih, H.C. Microstructure and Electrochemical Properties of High Entropy Alloys-a Comparison with Type-304 Stainless Steel. *Corros. Sci.* **2005**, *47*, 2257–2279. [[CrossRef](#)]
- Gludovatz, B.; Hohenwarter, A.; Catoor, D.; Chang, E.H.; George, E.P.; Ritchie, R.O. A Fracture-Resistant High-Entropy Alloy for Cryogenic Applications. *Science* **2014**, *345*, 1153–1158. [[CrossRef](#)] [[PubMed](#)]
- Cantor, B. Multicomponent High-Entropy Cantor Alloys. *Prog. Mater. Sci.* **2021**, *120*, 100754. [[CrossRef](#)]
- Lu, C.; Niu, L.; Chen, N.; Jin, K.; Yang, T.; Xiu, P.; Zhang, Y.; Gao, F.; Bei, H.; Shi, S.; et al. Enhancing Radiation Tolerance by Controlling Defect Mobility and Migration Pathways in Multicomponent Single-Phase Alloys. *Nat. Commun.* **2016**, *7*, 13564. [[CrossRef](#)] [[PubMed](#)]
- Granberg, F.; Nordlund, K.; Ullah, M.W.; Jin, K.; Lu, C.; Bei, H.; Wang, L.M.; Djurabekova, F.; Weber, W.J.; Zhang, Y. Mechanism of Radiation Damage Reduction in Equiatomic Multicomponent Single Phase Alloys. *Phys. Rev. Lett.* **2016**, *116*, 135504. [[CrossRef](#)] [[PubMed](#)]
- Ullah, M.W.; Aidhy, D.S.; Zhang, Y.; Weber, W.J. Damage Accumulation in Ion-Irradiated Ni-Based Concentrated Solid-Solution Alloys. *Acta Mater.* **2016**, *109*, 17–22. [[CrossRef](#)]
- Yang, L.; Chen, Y.; Miller, J.; Weber, W.J.; Bei, H.; Zhang, Y. Deformation Mechanisms in Single Crystal Ni-Based Concentrated Solid Solution Alloys by Nanoindentation. *Mater. Sci. Eng. A* **2022**, *856*, 143685. [[CrossRef](#)]
- Xiu, P.; Osetsky, Y.N.; Jiang, L.; Velisa, G.; Tong, Y.; Bei, H.; Weber, W.J.; Zhang, Y.; Wang, L. Dislocation Loop Evolution and Radiation Hardening in Nickel-Based Concentrated Solid Solution Alloys. *J. Nucl. Mater.* **2020**, *538*, 152247. [[CrossRef](#)]
- Gludovatz, B.; Hohenwarter, A.; Thurston, K.V.S.; Bei, H.; Wu, Z.; George, E.P.; Ritchie, R.O. Exceptional Damage-Tolerance of a Medium-Entropy Alloy CrCoNi at Cryogenic Temperatures. *Nat. Commun.* **2016**, *7*, 10602. [[CrossRef](#)]
- Zhang, Z.J.; Mao, M.M.; Wang, J.; Gludovatz, B.; Zhang, Z.; Mao, S.X.; George, E.P.; Yu, Q.; Ritchie, R.O. Nanoscale Origins of the Damage Tolerance of the High-Entropy Alloy CrMnFeCoNi. *Nat. Commun.* **2015**, *6*, 2–7. [[CrossRef](#)]
- Laplanche, G.; Kostka, A.; Reinhart, C.; Hunfeld, J.; Eggeler, G.; George, E.P. Reasons for the Superior Mechanical Properties of Medium-Entropy CrCoNi Compared to High-Entropy CrMnFeCoNi. *Acta Mater.* **2017**, *128*, 292–303. [[CrossRef](#)]
- Zhang, Z.; Sheng, H.; Wang, Z.; Gludovatz, B.; Zhang, Z.; George, E.P.; Yu, Q.; Mao, S.X.; Ritchie, R.O. Dislocation Mechanisms and 3D Twin Architectures Generate Exceptional Strength-Ductility-Toughness Combination in CrCoNi Medium-Entropy Alloy. *Nat. Commun.* **2017**, *8*, 14390. [[CrossRef](#)] [[PubMed](#)]
- Huang, H.; Li, X.; Dong, Z.; Li, W.; Huang, S.; Meng, D.; Lai, X.; Liu, T.; Zhu, S.; Vitos, L. Critical Stress for Twinning Nucleation in CrCoNi-Based Medium and High Entropy Alloys. *Acta Mater.* **2018**, *149*, 388–396. [[CrossRef](#)]
- Jin, K.; Lu, C.; Wang, L.M.; Qu, J.; Weber, W.J.; Zhang, Y.; Bei, H. Effects of Compositional Complexity on the Ion-Irradiation Induced Swelling and Hardening in Ni-Containing Equiatomic Alloys. *Scr. Mater.* **2016**, *119*, 65–70. [[CrossRef](#)]
- Zhang, Y.; Zhao, S.; Weber, W.J.; Nordlund, K.; Granberg, F.; Djurabekova, F. Atomic-Level Heterogeneity and Defect Dynamics in Concentrated Solid-Solution Alloys. *Curr. Opin. Solid State Mater. Sci.* **2017**, *21*, 221–237. [[CrossRef](#)]
- Yamakov, V.; Wolf, D.; Phillipot, S.R.; Mukherjee, A.K.; Gleiter, H. Dislocation Processes in the Deformation of Nanocrystalline Aluminium by Molecular-Dynamics Simulation. *Nat. Mater.* **2002**, *1*, 45–48. [[CrossRef](#)] [[PubMed](#)]
- Zhang, F.; Wu, Y.; Lou, H.; Zeng, Z.; Prakapenka, V.B.; Greenberg, E.; Ren, Y.; Yan, J.; Okasinski, J.S.; Liu, X.; et al. Polymorphism in a High-Entropy Alloy. *Nat. Commun.* **2017**, *8*, 15687. [[CrossRef](#)]
- Ding, J.; Yu, Q.; Asta, M.; Ritchie, R.O. Tunable Stacking Fault Energies by Tailoring Local Chemical Order in CrCoNi Medium-Entropy Alloys. *Proc. Natl. Acad. Sci. USA* **2018**, *115*, 8919–8924. [[CrossRef](#)]
- Lin, Q.; Liu, J.; An, X.; Wang, H.; Zhang, Y.; Liao, X. Cryogenic-Deformation-Induced Phase Transformation in an FeCoCrNi High-Entropy Alloy. *Mater. Res. Lett.* **2018**, *6*, 236–243. [[CrossRef](#)]

21. Zhao, S.; Stocks, G.M.; Zhang, Y. Stacking Fault Energies of Face-Centered Cubic Concentrated Solid Solution Alloys. *Acta Mater.* **2017**, *134*, 334–345. [[CrossRef](#)]
22. Zhao, S.; Osetsky, Y.; Stocks, G.M.; Zhang, Y. Local-Environment Dependence of Stacking Fault Energies in Concentrated Solid-Solution Alloys. *Npj Comput. Mater.* **2019**, *5*, 13. [[CrossRef](#)]
23. Niu, C.; LaRosa, C.R.; Miao, J.; Mills, M.J.; Ghazisaeidi, M. Magnetically-Driven Phase Transformation Strengthening in High Entropy Alloys. *Nat. Commun.* **2018**, *9*, 1363. [[CrossRef](#)] [[PubMed](#)]
24. Smith, T.M.; Hooshmand, M.S.; Esser, B.D.; Otto, F.; Mccomb, D.W.; George, E.P.; Ghazisaeidi, M.; Mills, M.J. Atomic-Scale Characterization and Modeling of 60° dislocations in a High-Entropy Alloy. *Acta Mater.* **2016**, *110*, 352–363. [[CrossRef](#)]
25. Zeng, Y.; Cai, X.; Koslowski, M. Effects of the Stacking Fault Energy Fluctuations on the Strengthening of Alloys. *Acta Mater.* **2019**, *164*, 1–11. [[CrossRef](#)]
26. Osetsky, Y.N.; Pharr, G.M.; Morris, J.R. Two Modes of Screw Dislocation Glide in Fcc Single-Phase Concentrated Alloys. *Acta Mater.* **2019**, *164*, 741–748. [[CrossRef](#)]
27. Zhao, S. Fluctuations in Stacking Fault Energies Improve Irradiation Tolerance of Concentrated Solid-Solution Alloys. *J. Nucl. Mater.* **2020**, *530*, 151886. [[CrossRef](#)]
28. Zhang, F.X.; Zhao, S.; Jin, K.; Xue, H.; Velisa, G.; Bei, H.; Huang, R.; Ko, J.Y.P.; Pagan, D.C.; Neufeind, J.C.; et al. Local Structure and Short-Range Order in a NiCoCr Solid Solution Alloy. *Phys. Rev. Lett.* **2017**, *118*, 205501. [[CrossRef](#)]
29. Zhang, R.; Zhao, S.; Ding, J.; Chong, Y.; Jia, T.; Ophus, C.; Asta, M.; Ritchie, R.O.; Minor, A.M. Short-Range Order and Its Impact on the CrCoNi Medium-Entropy Alloy. *Nature* **2020**, *581*, 283–287. [[CrossRef](#)] [[PubMed](#)]
30. Tuomisto, F.; Makkonen, I.; Heikinheimo, J.; Granberg, F.; Djurabekova, F.; Nordlund, K.; Velisa, G.; Bei, H.; Xue, H.; Weber, W.J.; et al. Segregation of Ni at Early Stages of Radiation Damage in NiCoFeCr Solid Solution Alloys. *Acta Mater.* **2020**, *196*, 44–51. [[CrossRef](#)]
31. Lu, C.; Yang, T.; Jin, K.; Gao, N.; Xiu, P.; Zhang, Y.; Gao, F.; Bei, H.; Weber, W.J.; Sun, K.; et al. Radiation-Induced Segregation on Defect Clusters in Single-Phase Concentrated Solid-Solution Alloys. *Acta Mater.* **2017**, *127*, 98–107. [[CrossRef](#)]
32. He, M.R.; Wang, S.; Shi, S.; Jin, K.; Bei, H.; Yasuda, K.; Matsumura, S.; Higashida, K.; Robertson, I.M. Mechanisms of Radiation-Induced Segregation in CrFeCoNi-Based Single-Phase Concentrated Solid Solution Alloys. *Acta Mater.* **2017**, *126*, 182–193. [[CrossRef](#)]
33. Koizumi, Y.; Nukaya, T.; Suzuki, S.; Kurosu, S.; Li, Y.; Matsumoto, H.; Sato, K.; Tanaka, Y.; Chiba, A. Suzuki Segregation in Co-Ni-Based Superalloy at 973 K: An Experimental and Computational Study by Phase-Field Simulation. *Acta Mater.* **2012**, *60*, 2901–2915. [[CrossRef](#)]
34. Zhao, S.; Egami, T.; Stocks, G.M.; Zhang, Y. Effect of d Electrons on Defect Properties in Equiatomic NiCoCr and NiCoFeCr Concentrated Solid Solution Alloys. *Phys. Rev. Mater.* **2018**, *2*, 013602. [[CrossRef](#)]
35. Kresse, G.; Furthmüller, J. Efficiency of Ab-Initio Total Energy Calculations for Metals and Semiconductors Using a Plane-Wave Basis Set. *Comput. Mater. Sci.* **1996**, *6*, 15–50. [[CrossRef](#)]
36. Perdew, J.P.; Burke, K.; Ernzerhof, M. Generalized Gradient Approximation Made Simple. *Phys. Rev. Lett.* **1996**, *77*, 3865–3868. [[CrossRef](#)]
37. Blöchl, P.E. Projector Augmented-Wave Method. *Phys. Rev. B* **1994**, *50*, 17953–17979. [[CrossRef](#)]
38. Methfessel, M.; Paxton, A.T. High-Precision Sampling for Brillouin-Zone Integration in Metals. *Phys. Rev. B* **1989**, *40*, 3616–3621. [[CrossRef](#)]
39. Cowley, J.M. Short-Range Order and Long-Range Order Parameters. *Phys. Rev.* **1965**, *138*, A1384. [[CrossRef](#)]
40. Cowley, J.M. An Approximate Theory of Order in Alloys. *Phys. Rev.* **1950**, *77*, 669–675. [[CrossRef](#)]
41. Van de Walle, A.; Asta, M.; Ceder, G. The Alloy Theoretic Automated Toolkit: A User Guide. *Calphad Comput. Coupling Phase Diagr. Thermochem.* **2002**, *26*, 539–553. [[CrossRef](#)]
42. Vítek, V. Intrinsic Stacking Faults in Body-Centred Cubic Crystals. *Philos. Mag.* **1968**, *18*, 773–786. [[CrossRef](#)]
43. Siegel, D.J. Generalized Stacking Fault Energies, Ductilities, and Twinnabilities of Ni and Selected Ni Alloys. *Appl. Phys. Lett.* **2005**, *87*, 121901. [[CrossRef](#)]
44. Bag, P.; Su, Y.C.; Kuo, Y.K.; Lai, Y.C.; Wu, S.K. Physical Properties of Face-Centered Cubic Structured High-Entropy Alloys: Effects of NiCo, NiFe, and NiCoFe Alloying with Mn, Cr, and Pd. *Phys. Rev. Mater.* **2021**, *5*, 29–31. [[CrossRef](#)]
45. Bleskov, I.; Hickel, T.; Neugebauer, J.; Ruban, A. Impact of Local Magnetism on Stacking Fault Energies: A First-Principles Investigation for Fcc Iron. *Phys. Rev. B* **2016**, *93*, 214115. [[CrossRef](#)]
46. Ogata, S.; Li, J.; Yip, S. Ideal Pure Shear Strength of Aluminum and Copper. *Science* **2002**, *298*, 807–811. [[CrossRef](#)]
47. Shang, S.L.; Wang, W.Y.; Zhou, B.C.; Wang, Y.; Darling, K.A.; Kecske, L.J.; Mathaudhu, S.N.; Liu, Z.K. Generalized Stacking Fault Energy, Ideal Strength and Twinnability of Dilute Mg-Based Alloys: A First-Principles Study of Shear Deformation. *Acta Mater.* **2014**, *67*, 168–180. [[CrossRef](#)]
48. Shang, S.L.; Zacherl, C.L.; Fang, H.Z.; Wang, Y.; Du, Y.; Liu, Z.K. Effects of Alloying Element and Temperature on the Stacking Fault Energies of Dilute Ni-Base Superalloys. *J. Phys. Condens. Matter* **2012**, *24*, 505403. [[CrossRef](#)]

49. Xin, H.; Vojvodic, A.; Voss, J.; Nørskov, J.K.; Abild-Pedersen, F. Effects of d -Band Shape on the Surface Reactivity of Transition-Metal Alloys. *Phys. Rev. B—Condens. Matter Mater. Phys.* **2014**, *89*, 115114. [[CrossRef](#)]
50. Li, H.; Draxl, C.; Wurster, S.; Pippal, R.; Romaner, L. Impact of d -Band Filling on the Dislocation Properties of Bcc Transition Metals: The Case of Tantalum-Tungsten Alloys Investigated by Density-Functional Theory. *Phys. Rev. B* **2017**, *95*, 094114. [[CrossRef](#)]

Disclaimer/Publisher's Note: The statements, opinions and data contained in all publications are solely those of the individual author(s) and contributor(s) and not of MDPI and/or the editor(s). MDPI and/or the editor(s) disclaim responsibility for any injury to people or property resulting from any ideas, methods, instructions or products referred to in the content.